frontiers in Earth Science

ORIGINAL RESEARCH
published: 21 February 2022
doi: 10.3389/feart.2022.813074

Distribution Prediction of Shale Deformation Structures in Tectonically Complex Area Based on Relationship Between Geological Structures and Shale Deformation

Guoxi Cheng[1,2], *Bo Jiang*[1,2]*, *Fengli Li*[1,2,3], *Ming Li*[1,2] *and Yu Song*[1,2]

[1]*Key Laboratory of Coalbed Methane Resource and Reservoir Formation Process, Ministry of Education, China University of Mining and Technology, Xuzhou, China,* [2]*School of Resources and Geosciences, China University of Mining and Technology, Xuzhou, China,* [3]*School of Resources and Civil Engineering, Suzhou University, Suzhou, China*

The alteration of shale structures and properties induced by tectonic activities is an important factor restricting the efficient utilization of shale gas resources. Predicting the distributions of shale deformation structures is of significance for the potential evaluation and favorable area optimization of shale resources in tectonically complex areas. Taking the Wufeng–Longmaxi shale of the southern Sichuan Basin as the research object, deformation observations of shale outcrops and shale core samples were conducted to reveal the distribution patterns of shale deformation structures in fault and fold structures. On this basis, the distribution rules of shale deformation structures in the unexposed areas were predicted by considering the structural framework of the study area. Our research indicated that faults can cause structural deformation in a limited area and that the influences of reverse faults were relatively more significant. Shale near the fault planes of reverse faults usually showed intense folding deformations, with well-developed bedding-parallel and crumpled cleavages. Strong deformation structures (crumpled, mylonitized, scaly, fractured-crumpled, and flaky structure) were distributed. Structural deformations in shale near normal faults were mainly characterized by the increase of tectonic fractures, and shale usually showed cataclastic structure. In the areas affected by strike-slip faults, bedding-perpendicular fractures and the fractures high-angle oblique to bedding planes were well developed. Folds can cause shale to deform in a larger area than faults. Shale in core zones usually displayed strong deformation structures. In the core–limb transitional areas of folds, shale mainly developed bedding-parallel and bedding-perpendicular fractures, and shale usually displayed platy and cataclastic structure. The observed structural deformations in fold limbs were generally weak, and shale usually showed primary structure and weak brittle deformation structures. According to the structural framework of the study area, it is predicted that strong deformation structures are mainly distributed in the core zones of anticlines (especially the tight and closed ones) and near the fault planes of large-scale reverse faults, while medium-intensity brittle deformation structures (platy and cataclastic structure) are distributed in core–limb transitional areas of anticlines and near the normal and strike-slip faults. In the limbs of

OPEN ACCESS

Edited by:
Jienan Pan,
Henan Polytechnic University, China

Reviewed by:
Xiaoshi Li,
Chinese Academy of Geological Sciences (CAGS), China
Hongjian Zhu,
Yanshan University, China
Fu Haijiao,
China University of Geosciences Wuhan, China

***Correspondence:**
Bo Jiang
jiangbo@cumt.edu.cn

Specialty section:
This article was submitted to Economic Geology, a section of the journal Frontiers in Earth Science

Received: *11 November 2021*
Accepted: *03 January 2022*
Published: *21 February 2022*

Citation:
Cheng G, Jiang B, Li F, Li M and Song Y (2022) Distribution Prediction of Shale Deformation Structures in Tectonically Complex Area Based on Relationship Between Geological Structures and Shale Deformation. Front. Earth Sci. 10:813074. doi: 10.3389/feart.2022.813074

anticlines and the areas controlled by synclines (mostly wide and gentle), shale mainly shows primary structure and weak brittle deformation structures.

Keywords: distribution prediction, shale deformation structures, organic-rich shale, geological structures, tectonically complex area

INTRODUCTION

With the continuous increase of proved shale gas resources and commercial utilization in recent years, research on the structure and physical properties of shale reservoirs is becoming a research hotspot in the field of unconventional natural gas geology. While evaluating the resource potential of shale gas, scholars noticed that the shale reservoirs in tectonically complex areas usually display structural deformation of varying properties and intensity (Guo and Zeng, 2015; Xiao et al., 2015; Zheng et al., 2018; Cheng et al., 2021). Moreover, porosity characterization showed that the tectonically deformed shale (TDS) exhibits distinct fracture and pore structures from the undeformed shale (Curtis, 2002; Eichhubl et al., 2005; Guo, 2013; Liang et al., 2017; Ma et al., 2014; Zhu et al., 2018), which affects the gas storage and seepage properties of shale reservoirs and leads to the strong heterogeneity of shale gas distribution in tectonically complex areas (Carey et al., 2015; Liang et al., 2020; Liu et al., 2012; Liu et al., 2016).

Although researchers paid much attention to various TDS in recent years, most of the research was independent and static and focused on the evolution rules of mineral composition, pore, and micro-fracture structures of various TDSs. The research objects include the Lujiaping Formation of the Lower Cambrian and the Liujiaping Formation of the Lower Carboniferous in the Daba mountain fold-thrust belt of the northeastern Sichuan basin (Ma et al., 2014; Zhu et al., 2018), the Longmaxi Formation of the Lower Silurian in the peripheral regions of the Sichuan basin (Liang et al., 2020; Li et al., 2021; Zhu et al., 2021), and the structurally complex belt of the northern Guizhou (Gu et al., 2020). The previous research generally supported the conclusion that the structural deformation of shale (especially brittle deformation) brought about abundant micro-fractures and made the pre-existing pores develop to form large connected pore structures. Thus, the pore structure connectivity and reservoir permeability were significantly enhanced (Liang et al., 2017; Liang et al., 2020; Zhu et al., 2018). However, different opinions existed in the evolution rules of pore structures of TDSs. Some scholars pointed out that tectonic compression caused the organic micro- and mesopores to collapse and made the intergranular pores closed, resulting in a decrease in the total porosity and gas adsorption capacity of TDSs (Liang et al., 2017; Ma et al., 2020; Gou et al., 2021; Li et al., 2021). However, it was also demonstrated that the strongly deformed shale exhibited a more developed micro- and mesopore structure (Ma et al., 2014; Ju et al., 2018; Zhu et al., 2019; Shang et al., 2020). These arguments suggest that deep and systematical study of the deformation characteristics and genetic mechanism of TDSs are required to reveal the true evolution rules of pore structures of TDSs.

In the newly published TDS research, the classification and deformation descriptions of TDSs usually referred to the relative findings in the field of tectonite and tectonically deformed coal (TDC). In a broad sense, scholars generally divided tectonite into cataclastic and mylonitized series (Sibson, 1977; Chester et al., 1985; Woodcock and Mort, 2008). Cataclastic series, or brittle deformation series, refers to the tectonically deformed rocks characterized by brittle fracture development and shale fragmentation, and the enhancement of structural deformation usually caused an increase in the density of tectonic fractures and fragmentation degree of shale blocks (Engelder, 1974). Mylonitized series, or ductile deformation series, is a type of tectonite formed by intracrystalline plastic rheology (intracrystalline and bicrystalline sliding), intergranular sliding and rotation, dynamic recrystallization, and the formation of new minerals (Sibson, 1977; Hatcher, 1978). The mylonitized tectonite is characterized by the obvious fine-grained shape and flow textures and is mostly belt-like distributed. Besides, some scholars also put forward the concept of brittle–ductile transitional series, which is a transitional deformation series between cataclastic and mylonitized series. The related concepts include "foliated cataclastic rock" and "semi-plastic mylonitized" (Chester et al., 1985; Marshark and Mitra, 1988; Zhong, 1994; Zhu and Wang, 1995). According to the widely accepted TDC classification, which took the deformation characteristics and genetic mechanism into account, TDCs were divided into three series, namely the brittle, ductile, and brittle-ductile transitional series (Jiang and Ju, 2004; Ju et al., 2004; Pan et al., 2015; Jiang et al., 2010; Li et al., 2019; Guoxi et al., 2020; Cheng et al., 2020a; Cheng et al., 2020b). The three TDC series were further divided into eight types, namely the cataclastic, porphyritic, granulitic, platy, scaly, crumpled, and mylonitized coal.

Similar to the tectonite and TDC classification, previous researchers put forward three shale deformation mechanisms: brittle, brittle-ductile transitional, and ductile deformation series (Ma et al., 2014; Ju et al., 2018; Zhu et al., 2018; Fengli et al., 2019; Li et al., 2021). Brittle deformation series is mainly displayed as the development of brittle fractures and the enhancement of shale fragmentation, corresponding to cataclastic tectonite and the brittle TDCs. It is worth noting that differences exist in the deformation mechanisms of ductile TDS and mylonitized tectonite. The study of tectonite mostly took the highly crystallized felsic rocks as the research objects, which are composed of large crystalline grains. However, the shale is essentially a type of fine-grained clastic rock and composed of fine mineral particles. As a result, under the ductile deformation environment (mostly characterized by high-temperature, high-confining pressure, and low strain rate), the tectonic stresses are more likely to release by intergranular sliding and grain rotation,

and it is difficult to maintain sufficient stress to produce obvious intra-crystalline plastic deformation in mineral grains. Consequently, the ductile deformed shale is mainly characterized by the intergranular sliding of fine mineral particles, accompanied by shale fragmentation and dynamic recrystallization on large mineral particles. In the research of Chen (1998), the deformation features of deformed fine-grained clastic rocks in the ductile shear zone with low-grade metamorphism were recorded and analyzed. Moreover, due to the well-developed foliation structure of shale, bedding slips were more likely to occur in shale than in other rocks under tectonic compressions, bringing about bedding-parallel fractures and cleavages. Thus, there are some predominated deformation structures in TDSs, such as platy, flaky, and scaly structure, and the strongly TDSs mostly are belt-like distributed along bedding planes.

There are noticeable differences in shale deformation in different structural locations, but only a few studies have been carried out to reveal the relationship between geological structures and shale deformation. Wang et al. (1982) recorded the deformation variations of tectonite within the southern fault zone of the Tancheng–Lujiang (Tan–Lu) fault belt. They found that the intensity of shale fragmentation largely decreased from the fault plane to the upper and lower sides, and the observed structural deformation gradually changed from brittle deformation to ductile deformation. Zhu et al. (2018) observed the shale deformation variations in the Liujiaping Formation of the Daba Mountain Thrust-fold belt (southeastern margin of the Sichuan basin). They found that there were mainly strongly brittle TDSs near the fault planes while the ductile TDSs were mainly distributed in the complex fold areas, and the intensity of shale deformation gradually decreased from core zones to limbs and from fault planes to fault sides. Deville et al. (2020) observed the deformation characteristics of a large-scale shale outcrop located in the Parras Basin of northeastern Mexico and identified deformation mechanisms of shale: penetrative ductile deformation and localized brittle deformation. Furthermore, they believed that the changes in pressure conditions could lead to the evolution of shale deformation mechanisms. In the research of Li et al. (2021), the structural styles of shale deformation were divided into four levels, from the weaker to the stronger, horizontal strata or monoclinic structures, simple and wide folds, complex and closed folds, and ductile shear zone. According to their finding, the undeformed shale gradually transits to the strongly deformed shale from level A to level D. To conclude, most of the research was performed to serve the sample collection, and few efforts have been made to predict the planar distribution of different TDSs based on the distribution and intensity of geological structures. Based on structural observation and modeling, Katori et al. (2021) constructed the rock deformation distribution patterns on the sides of the Median Tectonic Line (the largest onshore fault of Japan); their research showed that the rock deformation transit with the pattern of "strongly cataclasite, weakly cataclasite, ultramylonite, mylonite, protomylonite" and the tectonite of the same type were distributed in belts parallel to the main structural line.

As all tectonite is of tectonic origin, the formation and distribution of tectonite are significantly controlled by geological structures, and their influences on shale deformation vary with structural types and intensity. Thus, it should be an effective way to determine the distribution rules of shale deformation structures in unexposed areas by establishing the relationship between geological structures and shale deformation. A literature review shows that the current knowledge about shale deformation and the relationship between geological structure and shale deformation is insufficient, and it requires further study of shale deformation features on shale outcrops to reveal the controlling effects and mechanisms of geological structures on TDSs' distribution.

In this work, the southern Sichuan Basin, located in the junction area of the southern Sichuan low-steep fold belt and the Lou Mountain fold-thrust belt, was selected as the study area. With abundant shale outcrops and intense shale deformation, the southern Sichuan basin is an ideal region to study the distribution rules of shale deformation structures. Specifically, we systematically recorded the structural deformation features of shale outcrops and shale core samples to summarize the micro and macro deformation features of TDSs and reveal the controlling mechanisms of geological structures on shale deformation. Finally, we predicted the distribution rules of various shale deformation structures by considering the structural framework of the study area.

GEOLOGICAL SETTINGS

The Sichuan basin is located in the middle and east of the Sichuan Province of China, bounded by the Mian–Lue collision belt in the north, the Longmen Mountain fold-thrust belt in the west, the Qiyue Mountain fault in the east, and the Lou Mountain fold-thrust belt in the south (**Figure 1A**) (Burchfiel et al., 1995; Gu et al., 2021). The study area lies in the southern Sichuan low-steep fold belt (a secondary structural zone), which is bounded by the Huaying Mountain fault belt in the west, the Qiyue Mountain fault belt in the east, and the Gulin fault and its associated thrust faults in the south.

The strata exposed in the study area include Cambrian, Ordovician, Silurian, Permian, Triassic, Jurassic, and Middle–Upper Cretaceous (**Figures 1B,C**). There is no regionally distributed angular unconformity observed in the study area (Wei et al., 2019). Only two parallel unconformity systems were regionally distributed: one between the Silurian and Permian and the other between the Upper Jurassic and the Upper Cretaceous. The Wufeng Formation (O_3w) of the Upper Ordovician and the Longmaxi Formation (S_1l) of the Lower Silurian were mainly exposed near the cores and limbs of the N–S and E–W-extending anticlines in the middle and south region of the study area, which is strictly controlled by fold structures. The microscopic shale structure, organic geochemical, and mineralogical characteristics of the Wufeng-Longmaxi Formation are listed in **Supplementary Appendix SA**.

The southern Sichuan Basin mainly showed two structural systems: the near-E–W-trending structures and the near-N–S-trending structures (Cheng et al., 2021). The near-N–S-trending structures are mainly a series of synclines and anticlines with hinge lines inclined to the north. The N–S anticlines are relatively more

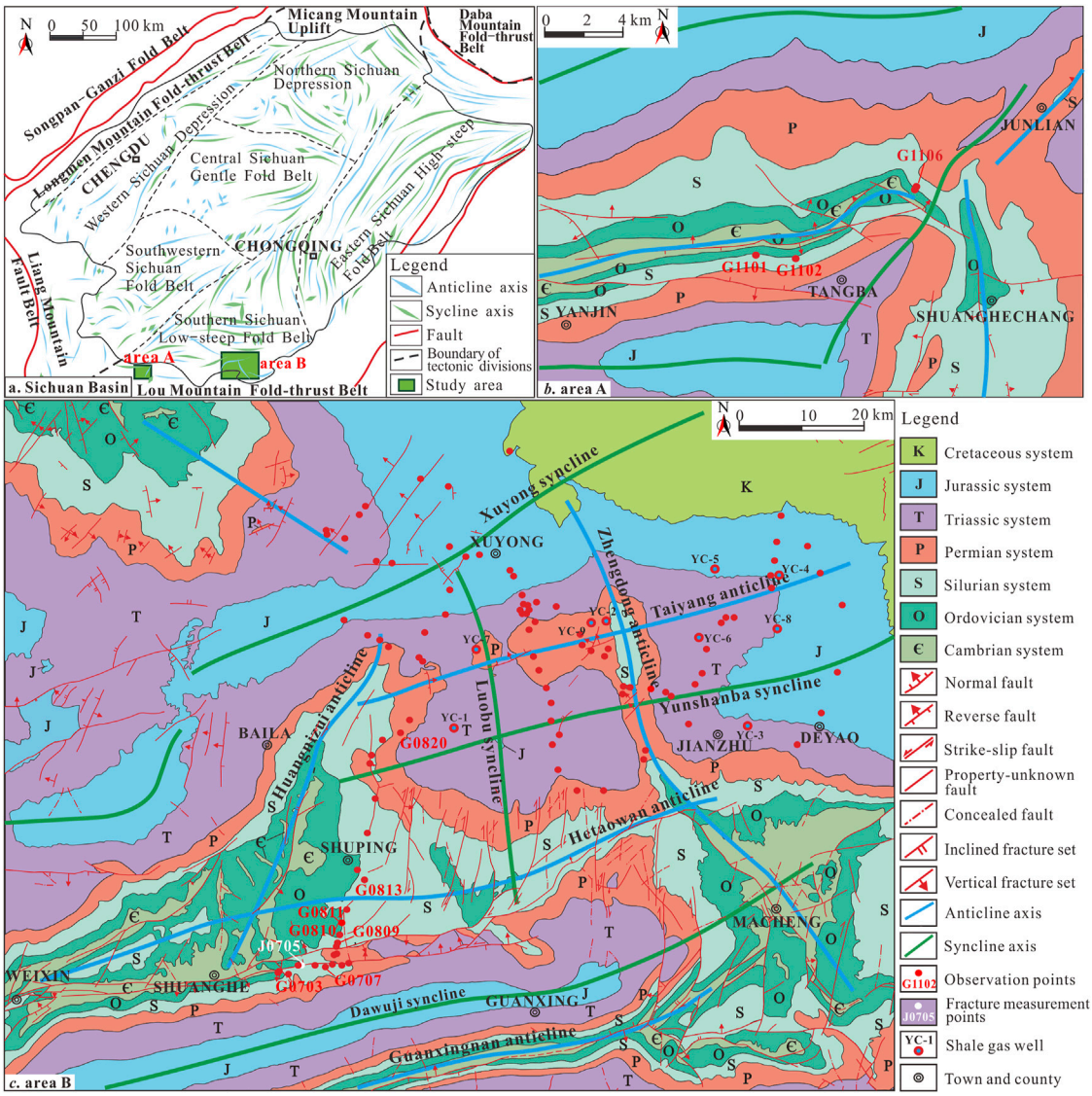

FIGURE 1 | Tectonic location **(A)** and structural outline map **(B,C)** of the study area.

closed than the N–S synclines. The near-E–W-trending structures are dominated by fold structures as well, and the folds distributed in the south are noticeably more complex and intense than those in the north. Besides, there are some near-E–W-trending strike faults developed in the south region, which mostly lies in the limbs of the E–W-trending anticlines.

During field surveys, we observed some structural features that indicate the formation and evolution sequence of the E–W and N–S compressive systems (Cheng et al., 2021): (a) the near-E–W-trending folds and reverse faults are mostly cut by the near-N–S-trending reverse faults; (b) the observed near-E–W-trending normal faults usually show the characteristics of "early reverse faults and later normal faults"; (c) the strata at the superposition areas of the two structural systems mostly dip the east or west. All these features indicate that the final finalization of the near-E–W-trending folds was later than that of the near-N–S-trending compressive structures. Our research team has carried out field studies and reconstructed the burial and thermal history of the Longmaxi Formation of the study area. The results showed that the peak period of the horizontal tectonic compression started after the Late Jurassic. The near-E–W-trending structures were finalized at the end of the Late Jurassic, while the near-N–S-trending structures were finalized at the end of the Oligocene (Cheng et al., 2021). These two periods of tectonic compressions generally determined the structural framework of the study area and then controlled the planar distribution of TDSs.

RESULTS AND DISCUSSION

We carried out shale outcrop observation during field study to reveal the control effects of geological structures on TDSs'

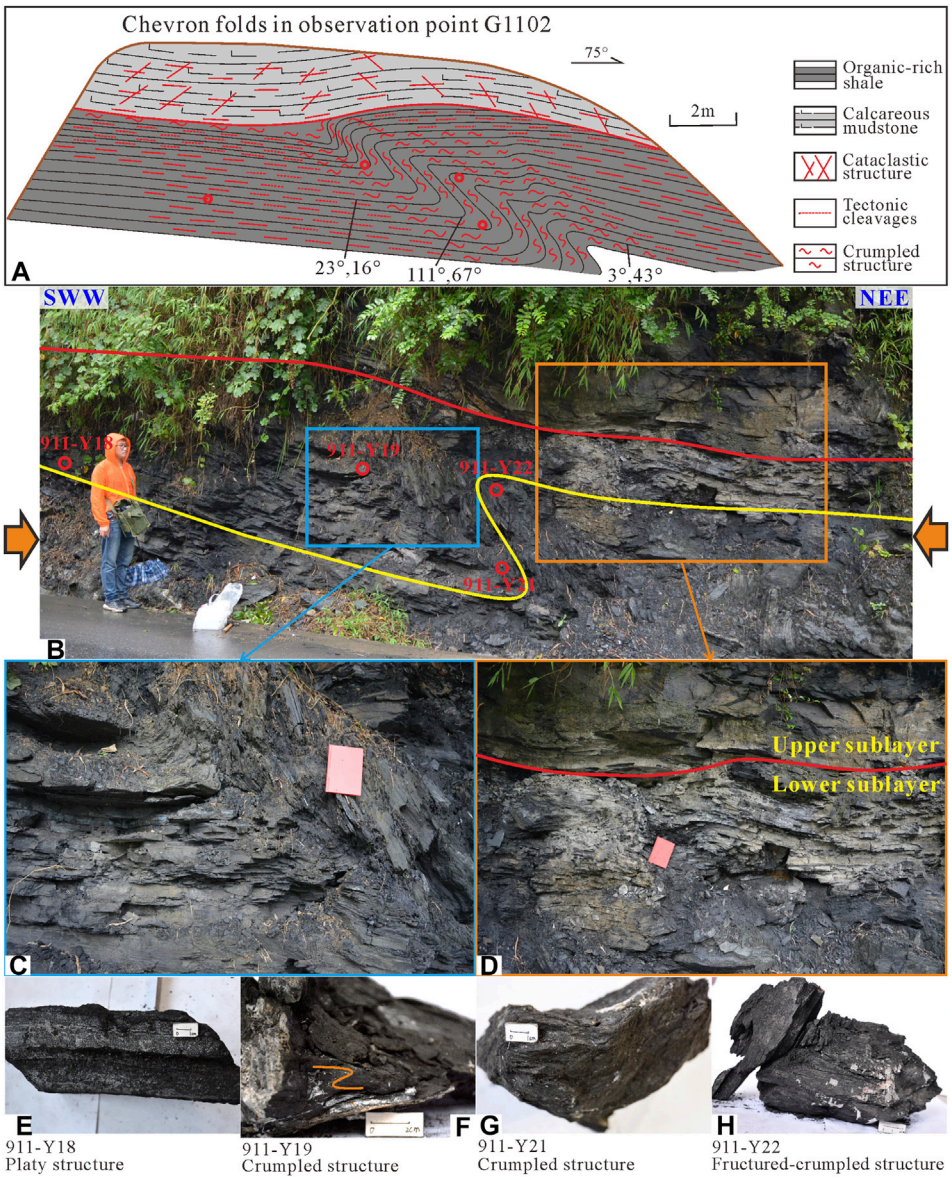

FIGURE 2 | Variations in shale deformation of the upper and lower sublayers of observation point G1102. Notes: all attitudes of areal structural elements are in "dip azimuth, dip angle" format in this paper. **(A,B)** the geological sketch map and field photograph, respectively; **(C)** the enlarged image of the small closed syncline; **(D)** the slip surface between the upper and lower sublayers; **(E-H)** the deformation features of shale samples with collection locations marked in A and B.

distribution. Specifically, we looked for shale outcrops with good observation and sampling conditions, observed and recorded the structural deformation characteristics of shale in different locations of geological structures, collected TDS samples, and conducted micro- and macro-deformation observations indoors, and then we summarized the controls of geological structures on shale deformation.

Referring to the classification scheme of tectonite and TDCs and considering the distinct deformation characteristics and genetic mechanisms of shale, we proposed a TDS classification scheme to standardize the description of shale deformation and to summarize the distribution rules of shale deformation structures. Three deformation series and eight deformation structures were distinguished from the collected shale samples: the brittle deformation series (including cataclastic, porphyritic, platy, and flaky structure), brittle–ductile transitional series (including fractured-cataclastic and scaly structure), and ductile series (including crumpled and mylonitized structure). The macro and micro deformation images and deformation characteristic descriptions of the whole series of TDSs can be found in **Supplementary Appendix SB**. This classification scheme corresponds well with the widely accepted classification scheme of tectonite (Sibson, 1977; Zhu and Wang, 1995) and TDCs (Jiang and Ju, 2004; Ju et al., 2004;

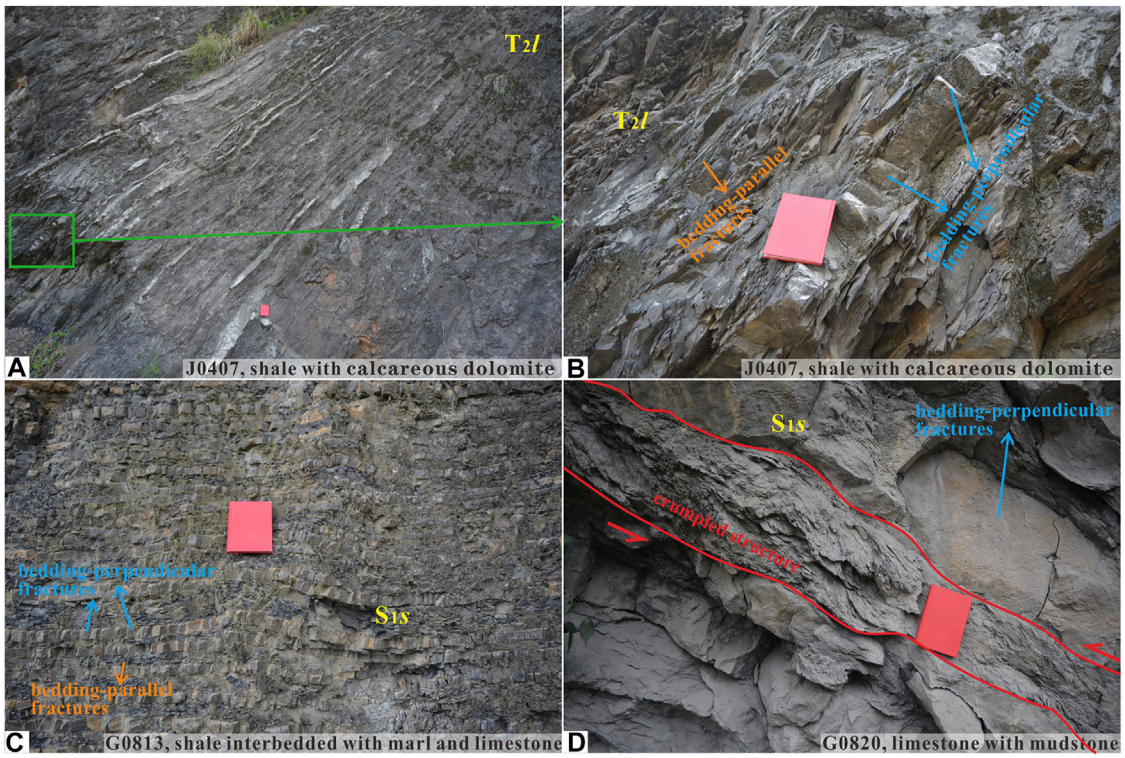

FIGURE 3 | Differences in tectonic fractures between soft and hard sublayers. Notes: **(A,B)** the observation point J0407, the Leikoupo Formation of the Middle Triassic (T_2l); **(C)** the observation point G0813, the Shiniulan Formation of the Lower Silurian (S_1s); **(D)** the observation point G0820, the S_1s Formation.

Jiang et al., 2010; Pan et al., 2015) and takes the distinct deformation characteristics of shale into account (Chen, 1998). The shale deformation characteristics in shale outcrops (with faults and/or folds exposed) were then observed and analyzed to reveal the controlling effects of different structural types on shale deformation. To make the distribution rules of TDSs more prominent and clearer, we illustrated the shale deformation characteristics on outcrops in the form of schematic diagrams.

Effects of Rock Properties and Rock Structures on Shale Deformation

During shale deformation observation on outcrops, we observed significant differences in shale deformation between different shale segmentations (with differences of mineral compositions and mechanical properties) of the same structural location.

An S-shaped fold (composed of a chevron anticline and syncline) was observed in the Longmaxi Formation of the observation point G1102 (**Figure 2**), which is located in the NWW limb of the Junlian–Tangba NNE-trending anticline. There were significant differences in shale deformation of the upper and lower shale sublayers. The thin-bedded dark shale of the lower sublayer experienced intense and complex folding deformation. Bedding-parallel cleavages and fractures were well developed, indicating intense bending sliding folding deformation. From core zones to limbs, shale deformation gradually changed from crumpled structure to flaky structure and then platy structure (**Figures 2A–C,E–H**,). In the thick-bedded mudstone of the upper sublayer, shale deformation was weaker and mainly showed cataclastic and platy structure (**Figure 2D**). Between the upper and lower sublayers, there developed a slip surface that fluctuated in a broad and gentle wave shape. The structural deformation of the shale near the slip plane was relatively stronger and gradually weakened to the direction away from the slip plane.

Figures 3A,B illustrate the fracture characteristics of outcrop J0407 located in the transitional area between the Xuyong syncline and the Taiyang anticline. The exposed strata are the dark gray thin-bedded shale and silty mudstone with thin-bedded calcareous dolomite of the Leikoupo Formation. The shale and silty mudstone mainly developed bedding-parallel fractures and fractures small-angle oblique to bedding planes, with a density of 120 m^{-1}. The fracture density in the shale near the dolomite can reach a maximum of 148 m^{-1}. On the contrary, the calcareous dolomite mainly developed bedding-perpendicular fractures with a density of 16 m^{-1}. In the dark gray carbonaceous mudstone thin-interbedded with grayish-yellow marl and limestone, there is a small flexure structure developed (**Figure 3C**). Bedding-parallel fractures were well developed in the thin-bedded mudstone, while in the marl and limestone, two groups of bedding-perpendicular fractures can be observed. **Figure 3D** showed a small bedding slip structure observed in the Qixia Formation. The mudstone interbedded within limestone experienced intense folding

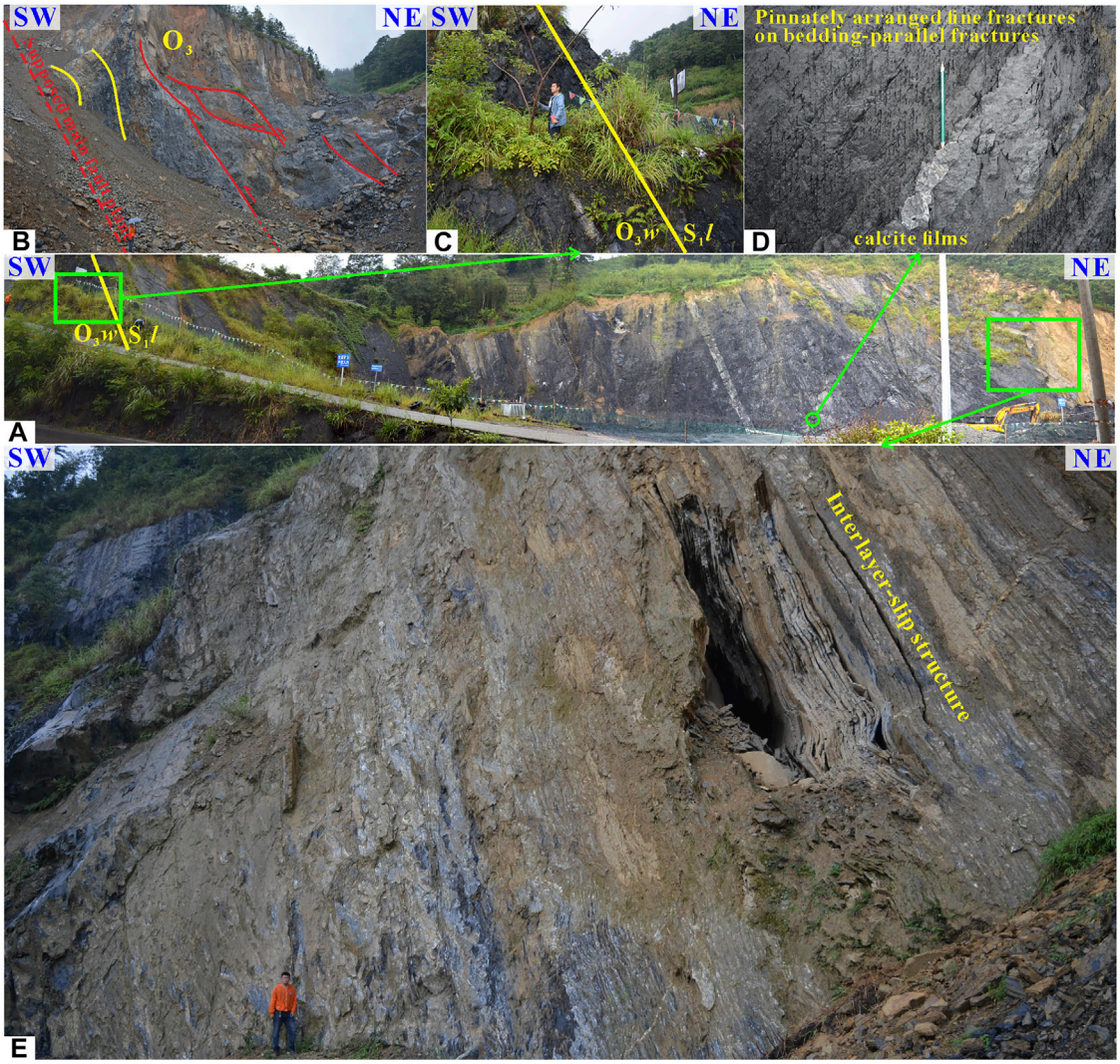

FIGURE 4 | Structural deformation characteristics of different sections of the Wufeng–Longmaxi Formation (observation point G1106). Notes: **(A)** a panorama of the Wufeng (O_3w) and Longmaxi Formation (S_1l); **(B)** secondary strike reverse faults and interlayer folds in the Middle and Upper Ordovician (O_{2-3}) limestone; **(C)** the O_3w Formation and the Lower member of the S_1l Formation; **(D)** bedding-parallel fractures in the Middle member of the S_1l Formation; **(E)** interlayer-slip structures in the Upper member of the S_1l Formation.

deformation, while the limestone showed weak structural deformation.

Figure 4 showed the structural deformations in different sections of the Wufeng–Longmaxi Formation. Observation point G1106 is located in the NE limb of an NW extending closed anticline and exposed the Middle and Upper Ordovician (O_{2-3}), Wufeng Formation (O_3w), and Longmaxi Formation (S_1l). Affected by the NW-trending anticline, the strata generally inclined to the NE direction, and the dip angle was generally larger than 60° (**Figure 4A**). There were secondary strike reverse faults and interlayer folds developed in the O_{2-3} limestone (**Figure 4B**), indicating the intense tectonic compression from northeast to southwest. The Wufeng Formation and the lower member of the Longmaxi Formation mostly showed platy and cataclastic structure (**Figure 4C**). The structural deformation was mainly characterized by the bedding-parallel and bedding-perpendicular tectonic fractures, most of which were filled with calcite films (**Figure 4D**). In the calcareous shale of the upper section of the Longmaxi Formation, which was thin-interbedded with silty mudstone and marl, detachment structures were stably developed and showed platy structure (**Figure 4E**). The structural deformation features at the observation point G1106 indicated that the shale deformation at fold limbs is relatively weaker and mainly dominated by brittle deformation (tectonic fractures). In sections with homogeneous mineral composition, shale tends to show platy and cataclastic structure, while in the thin-interbedded sections, tectonic compressions tend to cause bedding slips and form platy structure.

The observation point J0705 is located near the fault plane of a secondary reverse fault in the south limb of the NEE-trending

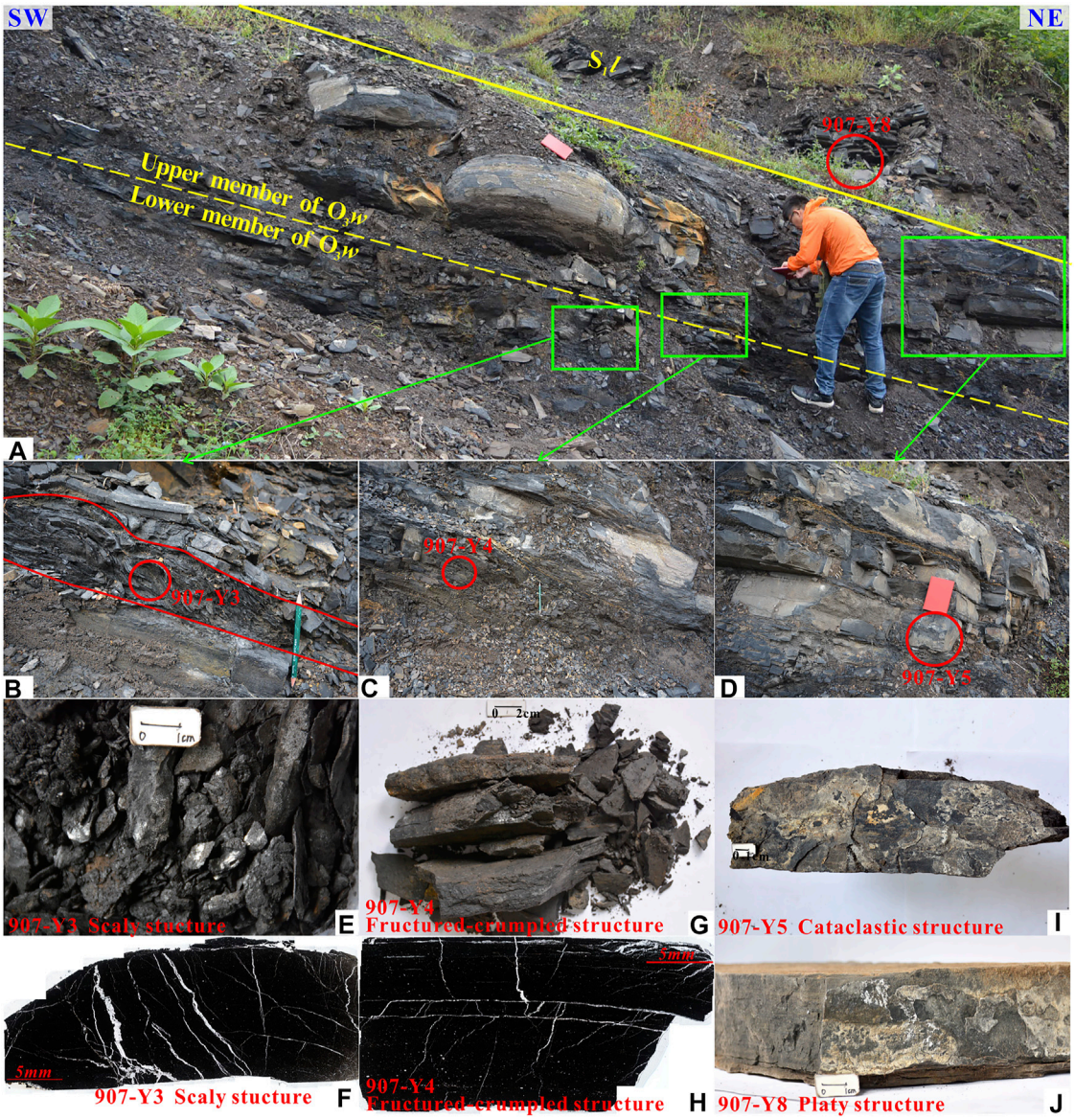

FIGURE 5 | Shale deformation characteristics of the Wufeng–Longmaxi Formation in observation point J0705. Notes:**(A)** a panorama of the Wufeng (O_3w) and Lower member of the Longmaxi Formation (S_1l); **(B,C)** the lower member of the O_3w Formation; **(D)** the Upper member of the O_3w Formation; **(E-J)** macro and micro deformation features of shale samples with collection locations marked in A-D.

Hetaowan anticline (**Figure 5**). The Wufeng Formation and the lower member of the Longmaxi Formation were exposed (**Figure 5A**). The Wufeng Formation in this observation point consists of upper and lower members, and significant differences existed in the structural deformation characteristics of the two members. The black thin-bedded shale of the lower member of the Wufeng Formation showed intense structural deformation (mainly developed flaky–and platy structure), with dense bedding-parallel fractures stably developed (**Figures 5B,C**). A sliding deformation belt was observed near the upper member of the Wufeng Formation (usually referred to as the Guanyinqiao member), with a thickness of about 20 cm (**Figure 5B**). Shale in the strong deformation belt usually showed as scaly or thin lens-shaped blocks, which were usually covered by bright and smooth friction surfaces (**Figures 5E–H**). The existence and deformation features of the strong deformation belt indicate that a noticeable bedding-parallel slip has occurred near the contact section of the lower and upper members of the Wufeng Formation. The upper member of the Wufeng Formation consists of medium–thick-bedded dark-gray shale that showed weak structural deformation. Shale mostly displayed cataclastic and platy structure, with bedding-parallel and bedding-perpendicular tectonic fractures well developed (**Figures 5D,I**).

The thin-bedded shale at the bottom member of the Longmaxi Formation mainly developed bedding-parallel fractures and less developed bedding-perpendicular fractures (**Figure 5J**), and the

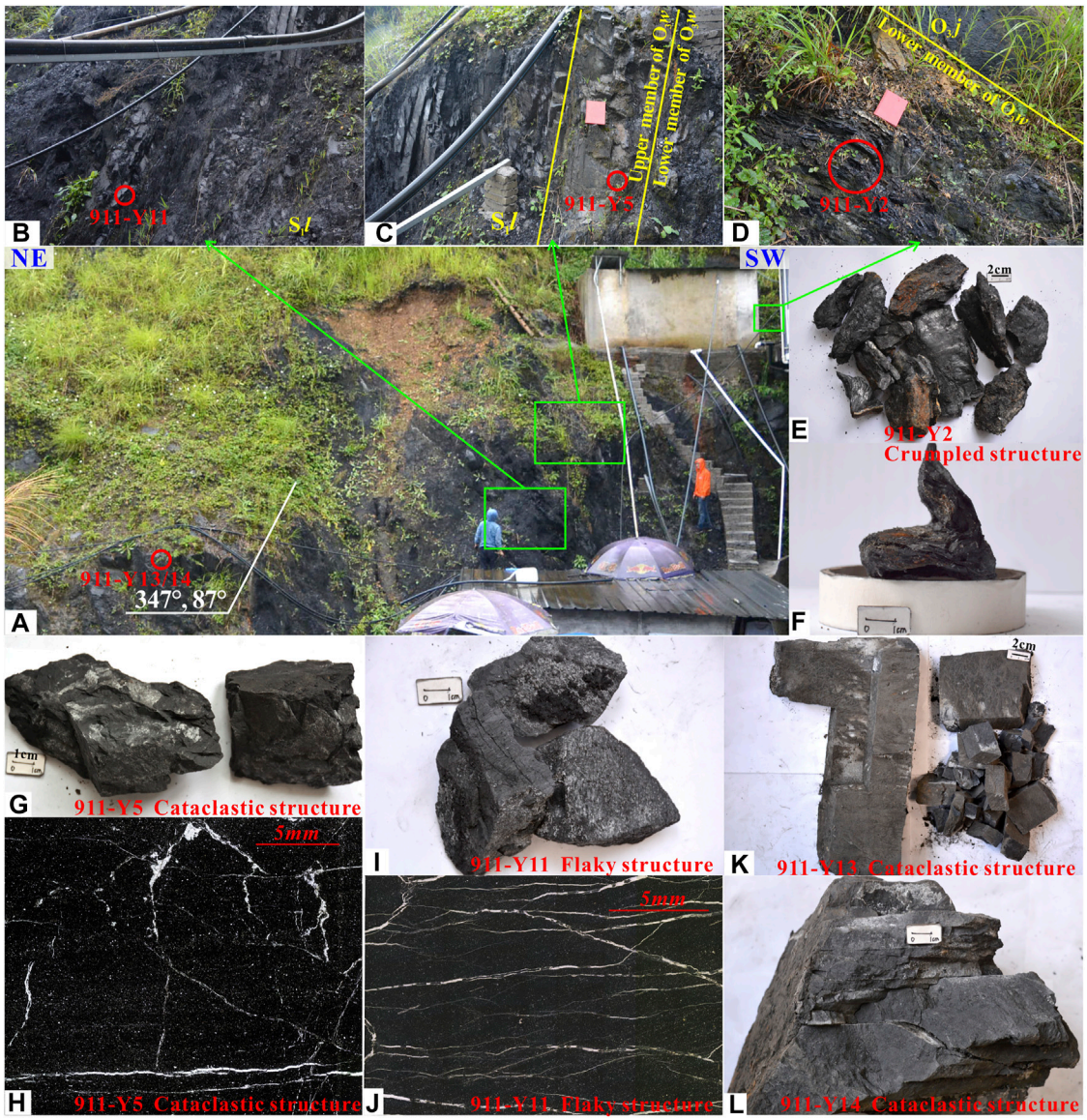

FIGURE 6 | Variations in shale deformation of different segmentation of the Wufeng–Longmaxi Formation (observation point G1101). Notes: **(A)** a panorama of the Wufeng (O_3w) and Longmaxi (S_1l) Formation; **(B)** the Lower member of the S_1l Formation; **(C,D)** the Upper and Lower member of the O_3w Formation; **(E-L)** macro and micro deformation features of shale samples with collection locations marked in A-D.

fracture density was higher than that of the upper member of the Wufeng Formation.

In summary, the lower member of the Wufeng Formation and the bottom member of the Longmaxi Formation generally showed stronger structural deformation, which are located at the bottom and top of the medium–thick-bedded calcareous shale (the upper member of the Wufeng Formation). These strong deformation belts indicated that bedding slips are more likely to occur at the junction section of the strong sublayers (usually thick-bedded shale with high calcium content) and weak sublayers (thin-bedded shale with high organic content).

Observation point G1101 is located in the core–limb transitional area of a NEE-trending closed anticline, with the strata attitude of 347°, 87°. There is a near-E–W-trending reverse fault developed in the core of the anticline (**Figure 1**), indicating strong N–S-trending structural deformations. The Wufeng–Longmaxi Formation exposed in this outcrop showed strong structural deformations, but significant differences existed in shale deformation of different sections (**Figure 6A**).

In the bottom member of the Wufeng Formation, the thin-bedded shale showed intense folding deformation (**Figures 6D–F**): shale usually displayed as irregularly crumpled, lenticular, and flaky blocks, and shale blocks were mostly covered by smooth friction surfaces. There was a bedding slip in the bottom of the Wufeng Formation. The lower member of the Wufeng Formation was strongly deformed and mainly

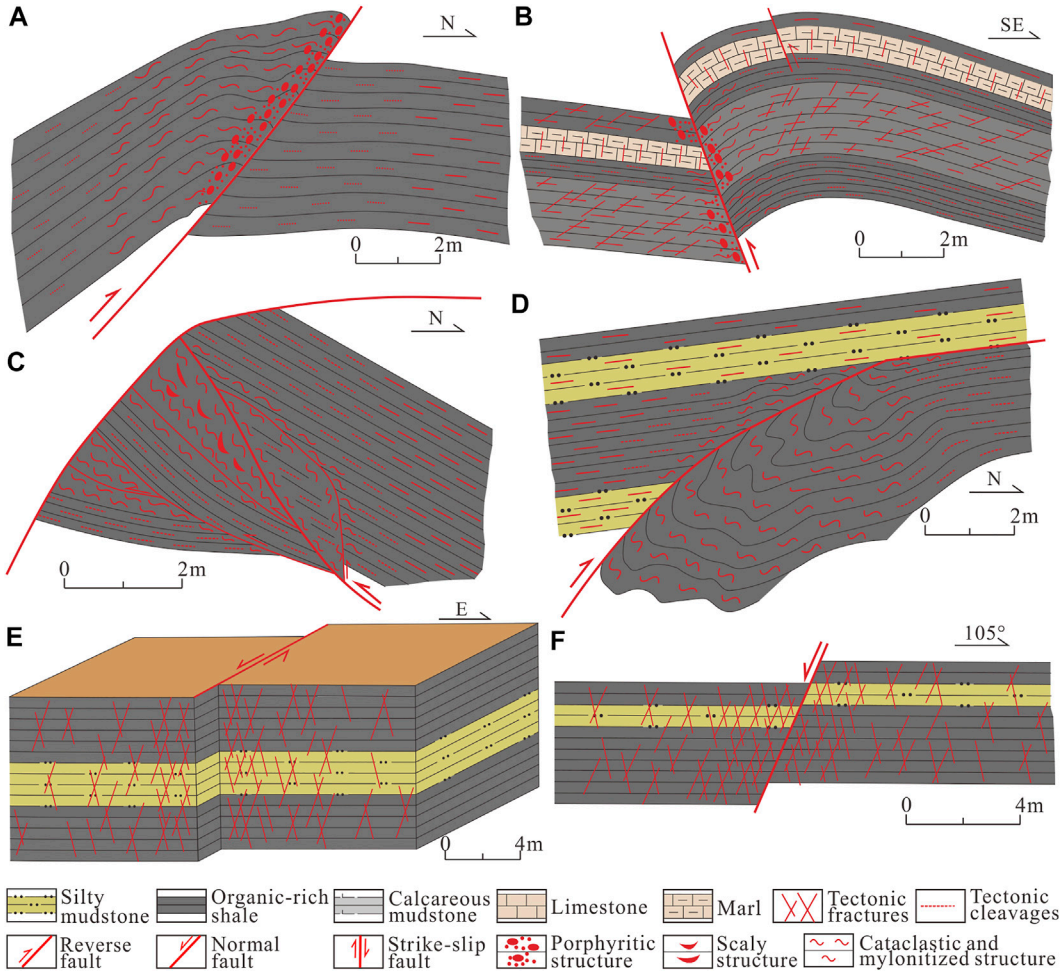

FIGURE 7 | Distribution schematic diagrams of shale deformation structures in fault structures. Notes: **(A)** a reverse fault in observation point G0810; **(B)** a reverse fault in observation point G0703; **(C)** a reverse fault in observation point G0707; **(D)** a reverse fault in observation point G0809; **(E)** a strike-slip fault in observation point G0811; **(F)** a normal fault in fracture measurement point J0705.

developed flaky, scaly, and crumpled structure (**Figures 6D–F**), while the upper member (the Guanyinqiao member) mainly showed cataclastic structure (**Figures 6C,G,H**).

The lower member of the Longmaxi Formation showed intense structural deformation as well, with dense and fine tectonic fractures well developed. The displacement traces can be observed on the large blocks. Shale generally showed flaky and porphyritic structure interbedded with platy structure (**Figures 6B,I,J**). From the lower member of the Longmaxi Formation to the upper member, shale gradually transited into platy and cataclastic structure (**Figures 6K,L**).

To conclude, the strongest structural deformation (porphyritic, flaky, scaly, and crumpled structure) usually occurred in the lower member of the Wufeng Formation and the lower member of the Longmaxi Formation, which are both dominated by thin-bedded shale. The upper member of the Wufeng Formation and the middle–upper member of the Longmaxi Formation showed relatively weaker deformation structures, such as platy, cataclastic structure.

Based on the comparative analysis of shale deformation on the above shale outcrops and the shale cores from nine shale gas evaluation wells in the study area (Cheng et al., 2021), it is found that the strong deformation structures and bedding slip planes were mainly distributed in these three sections: the bottom member of the Wufeng Formation near the underlying limestone, the bottom member of the Longmaxi Formation near the upper member of the Wufeng Formation, and the upper member of the Longmaxi Formation (thin-bedded shale interbedded with marl and silty mudstone). Under intense tectonic compressions, detachment structures were easier to occur in these three sections, resulting in the ductile, brittle–ductile transitional deformation structures (such as crumpled, scaly, flaky structure) in the lower member of the Wufeng Formation and the lower member of the Longmaxi Formation. As bedding sliding deformation mostly displayed as small-scale slip structures in the interfaces of laminas, shale in the upper member of the Longmaxi Formation usually showed platy structure. As for the upper member of the Wufeng

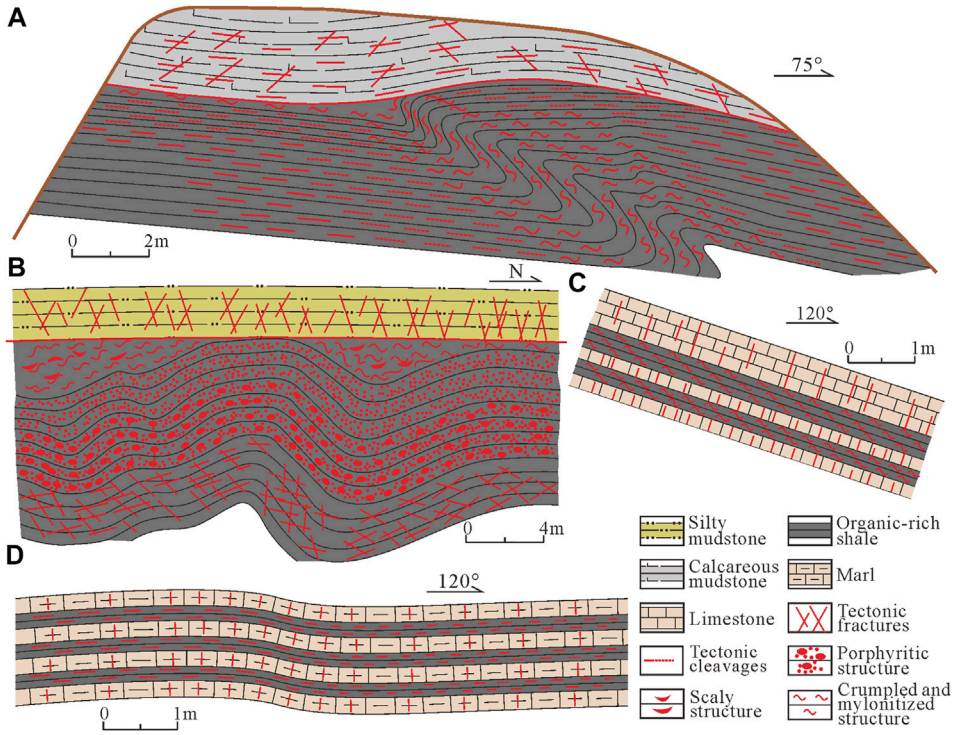

FIGURE 8 | Distribution schematic diagrams of shale deformation structures in fold structures. Notes: **(A)** chevron folds in observation point G1102; **(B)** folds in observation point G0811; **(C)** small bedding slip structures in observation point G0820; **(D)** a flexure structure in observation point G0813.

TABLE 1 | Shale deformation characteristics in different structural locations.

	Thin-bedded shale sections (the lower member of the Wufeng Formation and the lower member of the Longmaxi Formation)	Medium–thick-bedded shale sections (the upper member of the Wufeng Formation and the middle and upper members of the Longmaxi Formation)
Fold cores	Crumpled, mylonitized, fractured-crumpled, scaly, and porphyritic structure showing complex folding deformation. Shale deformation structures can display two zoning patterns: vertical zoning pattern (to the direction away from the main slip surfaces, shale transited from crumpled, mylonitized, and scaly structure to porphyritic and cataclastic structure), horizontal zoning pattern (from axial surfaces to the outside, shale gradually changes from crumpled, fractured-crumpled, and scaly structure to flaky and then platy structure)	Dominated by platy and cataclastic structure. Stably develop bedding-parallel tectonic fractures and partially fractures perpendicular to and oblique to bedding planes
Fold limbs	Platy and flaky structure with bedding-parallel fractures and compressive–shear fractures oblique to bedding planes	Weak structural deformation; dominated by weakly deformed cataclastic structure and primary structure. Fractures are mostly perpendicular to or large-angle oblique to bedding planes
Reverse faults	Mainly develop crumpled, scaly, and flaky structure; partially develop porphyritic structure near the fault planes of high-angle reverse faults. Bedding-parallel and crumpled cleavages are well developed. As the distance from fault planes increases, shale generally transits from ductile and brittle–ductile transitional deformation to brittle deformation and the intensity of brittle deformation gradually decreases	Platy and cataclastic structure with bedding-perpendicular and bedding-parallel tectonic fractures well-developed
Strike-slip faults	Cataclastic structure with tectonic fractures perpendicular to or high-angle oblique to bedding planes. Influences on shale deformation are relatively limited, and shale rapidly changes from cataclastic structure near the fault planes into primary structures in two walls of strike-slip faults	Cataclastic and primary structure. Structural deformation is generally slighter than that of the thin-bedded shale sections
Normal faults	Cataclastic structure; mainly tensile fractures. From fault planes to two walls of faults, shale gradually transits from cataclastic structure to primary structure	Cataclastic and primary structure with weak structural deformation

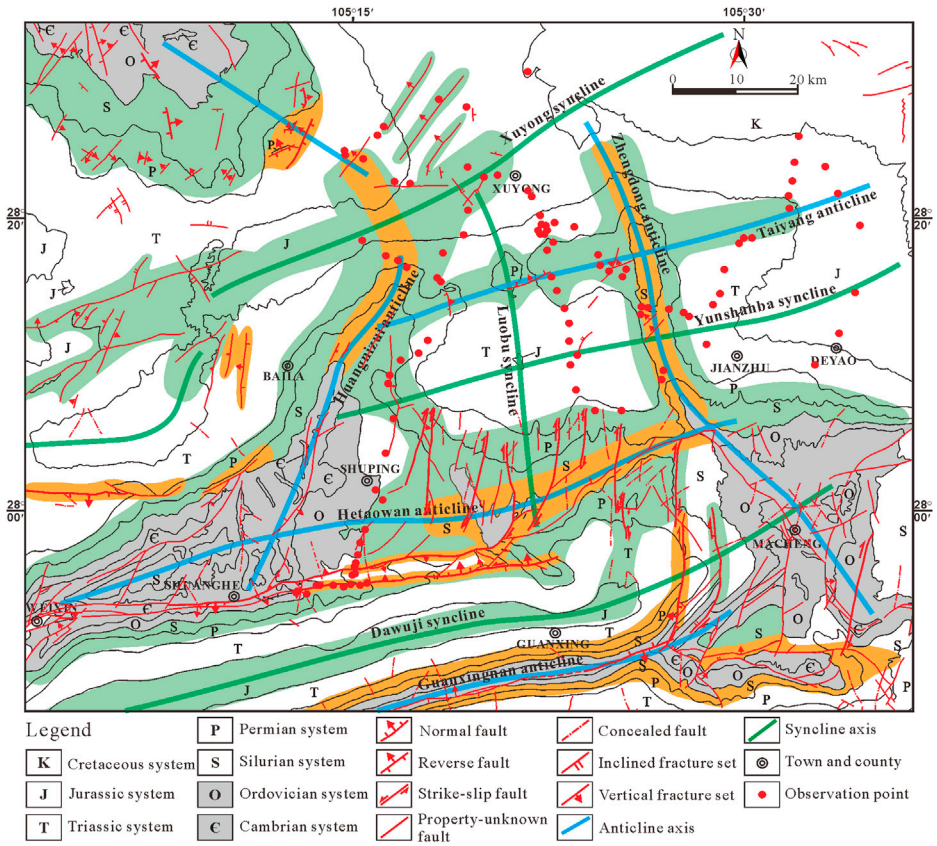

FIGURE 9 | Predicted distribution rules of different shale deformation structures. Notes: Light green areas develop medium-intensity brittle deformation structures, such as cataclastic and platy structure. Orange areas develop strong deformation structures, such as porphyritic, flaky, fractured-crumpled, scaly, and crumpled, and mylonitized structure. Gray areas means the eroded areas of the Wufeng–Longmaxi Formation. White areas develop primary structure and weak brittle deformation structures.

Formation and the middle member of the Longmaxi Formation, shale deformation was mainly characterized by developing large-scale bedding-parallel and bedding-perpendicular tectonic fractures, and shale usually showed cataclastic and platy structure.

Effects of Faults on Shale Deformation

Generally, the influences of faults on shale deformation were relatively slighter than that of folds, and the effects of reverse faults were more significant than that of normal and strike-slip faults.

Figure 7A (observation point J0810) illustrates a small secondary reverse fault that lies in the core zone of the NEE-trending Hetaowan anticline. In the ganging wall block near the fault plane, shale generally showed the porphyritic structure. As the distance from the fault plane increases, shale gradually transited from porphyritic structure to crumpled, flaky, and platy structure. Not far away from observation point J0810, observation point G0809 (**Figure 7B**) showed a reverse fault with a large dip, where gray-black thin-bedded shale, grayish-yellow calcareous mudstone, and marl were exposed. The thin-bedded shale near the fault plane generally showed crumpled and mylonitized structure and gradually transited into flaky structure and then platy structure. The calcareous mudstone and marl near the fault plane mainly displayed porphyritic structure and less developed crumpled structure. To the direction away from the fault plane, shale successively showed cataclastic and platy structure. The porphyritic structure was both observed near the fault planes of reserved faults shown in **Figures 7A,B**.

In the areas controlled by low-angle reverse faults, shale displayed different deformation characteristics. Ductile and brittle–ductile transitional deformation structures (such as crumpled, mylonitized, fractured-crumpled, and scaly structure) are relatively more widely developed. **Figure 7C** (observation point G0707) illustrates a series of small reverse faults found near the E–W-trending reverse fault in the core of the Hetaowan anticline. The shale near the fault planes showed strong deformation (mainly crumpled, mylonitized, scaly, and flaky structure) and gradually changed to flaky, cataclastic, and platy structure. **Figure 7D** (observation point G0703) shows a small reverse fault in silty mudstone and shale. The main fault plane gradually changed from oblique-to-beddings to parallel-to-bedding from the south to the north, and the medium–thick-bedded silty mudstone in the hanging wall was pushed to the upside of the shale in the footwall, indicating that the hanging wall experienced long-distance movement. The silty mudstone

showed weak structural deformation, dominated by weakly cataclastic and primary structure. The shale near the fault plane has experienced intense and complex folding deformations, manifested in crumpled and mylonitized structure. To the direction away from the fault plane, shale gradually transited to flaky and platy structure.

In summary, the thin-bedded shale near the reverse faults usually deformed in the form of folding deformation, bedding-parallel and crumpled cleavages and showed crumpled, mylonitized, fractured-crumpled, scaly, and flaky structure. Porphyritic structure was sometimes observed near the fault planes of high-angle reverse faults. With the increase of the distance from fault planes, shale deformation generally transited from ductile and brittle–ductile transitional deformation to brittle deformation, and the deformation intensity gradually decreased (cataclastic structure changed into platy structure, and the density of tectonic fractures decreased). Moreover, the shale in the hanging walls of reverse faults generally showed stronger structural deformation. The exception existed when there were hard sublayers near fault planes (such as marl and silty mudstone). In this case, the stronger structural deformation (maybe not in the hanging wall) usually appeared in the thin-bedded shale. The relatively hard layers, however, usually showed weak deformation structures, such as platy and cataclastic structure.

Compared with reverse faults, strike-slip faults and normal faults have relatively slighter influences on shale deformation. Shale near strike-slip faults mainly showed brittle deformation structure, characterized by tectonic fractures near perpendicular to or high-angle oblique to bedding planes. The intensity of brittle deformation rapidly decreased to the direction away from the fault planes. In the observation point G0811 (**Figure 7E**), we observed a strike-slip fault, where the thin-bedded shale and silty mudstone largely exhibited the same deformation characteristics (the shale was more significantly deformed than the silty mudstone). From the fault plane to the fault sides, shale gradually changed from cataclastic structure to primary structure.

In the areas near the fault planes of normal faults, shale deformation was mainly characterized by the increase of tectonic fractures, which is dominated by the derived tensile fractures perpendicular to bedding planes. Shale mostly showed cataclastic and primary structure. **Figure 7F** illustrated a small normal fault, where the shale near the fault plane mainly showed cataclastic structure and rapidly transited into primary structure as away from the fault plane.

Effects of Folds on Shale Deformation

Folds generally caused shale deformation in a larger area than faults, and the distribution of deformation structures usually showed more considerable variations in different lithologic segmentations.

The thin-bedded shale near fold cores usually showed intense and complex longitudinal folding deformations, with bedding-parallel and crumpled cleavages and fractures well developed. Shale blocks mostly showed tight arc and crumpled shapes and were covered by smooth and intact friction surfaces, forming crumpled, scaly, fractured-crumpled, and porphyritic structure (**Figures 8A,B**). Moreover, the thin-bedded shale near the hard sublayers generally displayed the strongest deformation structures (such as crumpled, mylonitized, and scaly structure), and the shale migrated to structural spaces in the form of solid rheology. Under the effects of bedding slip and bedding flow deformations, the thin-bedded silty mudstone and marl intercalated in the thin-bedded shale were usually pulled apart.

Due to the differences in strata structure, the distributions of shale deformation structures can show two zoning patterns: horizontal distribution pattern (pattern A) and vertical distribution pattern (pattern B).

Pattern A: The folds are tight and closed (as illustrated in **Figure 8A**). In this case, the distribution of deformation structures showed zoning characteristics from core zones to limbs. Shale in fold cores mostly exhibited ductile and brittle–ductile transitional deformation structures (mainly crumpled, fractured-crumpled, and scaly structure). However, shale in limbs usually showed platy–and flaky structure (brittle deformation structures).

Pattern B: The folds are wider and broader, as illustrated in **Figure 8B**. Under this condition, folds mostly caused shale deformation in a significantly larger area than pattern A. The deformation structures were distributed in belts. The distribution belts of deformation structures were in accordance with the entire shape of the deformation zone. To the direction away from the slip surfaces, shale gradually changed from ductile and brittle–ductile transitional deformation structures into brittle ones (mainly porphyritic and cataclastic structure). Shale deformation of the thick-bedded shale segmentations was noticeably weaker than that of the thin-bedded shale, characterized by the development of tectonic fractures (dominated by bedding-parallel fractures and less developed fractures oblique to bedding planes; **Figures 8A,B**).

In the limbs of fold structures, longitudinal folding deformations were relatively slighter and mostly showed as interlayer sliding deformations. The structural deformation of the thin-bedded shale was usually displayed as the development of bedding-parallel fractures, causing platy and flaky structure. The density of tectonic fractures usually reached the maximum in the segmentations contact with hard sublayers. Besides, in partial areas, there developed compressive–shear fractures oblique to bedding planes at an acute angle (**Figure 3B**), which were derived from the shear stresses during bedding slips.

Figures 8C,D illustrate the deformation features of two outcrops located in the limbs of large-scale folds, developed with thin-interbedded shale and limestone and shale and marl, respectively. Noticeable differences in structural deformation were observed between the hard and weak sublayers. The thin-bedded shale mainly experienced bedding sliding deformations, leading to the bedding-parallel or crumpled fractures and cleavages. Shale mainly exhibited crumpled, scaly, and flaky structure. In hard sublayers, such as marl and limestone, shale deformations were mainly characterized by the development of tectonic fractures perpendicular to bedding planes, and the fracture density is generally negatively correlated with the thickness of fractured sublayers. In the research of Cheng et al. (2021), negative power

functions were observed between the density of tectonic fractures and the thickness of fractured sublayers.

Shale Deformation Prediction Based on Geological Structures

Geological structures truthfully recorded the direction, form, and intensity of the experienced tectonic actions. It should be an effective way to predict the deformation characteristics and distribution laws of various types of TDSs in the unexposed areas based on the relationship between geological structures and shale deformation. In this work, we summarized the influencing modes of geological structures on shale deformation based on shale outcrop observations (**Table 1**) and then predicted the regional and longitudinal distributions of different TDSs (**Figure 9**).

The influences of normal faults and strike-slip faults on shale deformation are relatively limited and mainly characterized by the increase of tectonic fractures. The induced fractures are mostly perpendicular to or oblique to bedding planes at a large angle. Shale near the fault planes usually exhibited cataclastic structure, and the intensity of shale deformation rapidly decreased with the increase of distance from fault planes.

The thin-bedded shale near the fault planes of reverse faults usually experienced folding deformations with well-developed bedding-parallel and crumpled cleavages, showing strong deformation structures. Strong brittle deformation structures were observed in a small range near the fault planes of high-angle reverse faults. With the increase of the distance from fault planes, the structural deformation of shale generally showed the transition trends of "from ductile and brittle–ductile deformation to brittle deformation" and "from strong brittle deformation structures to weak brittle deformation structures and then primary structure." The relatively hard layers (medium–thick-bedded shale, silty mudstone, and marl) near reverse faults mostly experienced weak structural deformation and showed platy and cataclastic structure, developing mainly bedding-perpendicular and bedding-parallel fractures and less fractures oblique to bedding planes.

Near the core zones of folds and the superposition areas of folds of different directions, the thin-bedded shale usually showed complex folding deformations and displayed crumpled, fractured-crumpled, scaly, and porphyritic structure, with bedding-parallel and crumpled cleavages stably and densely developed. Due to the differences in shale's brittleness, structural deformation structures can show two zoning patterns. The vertical zoning pattern (shale deformation structures zoning along bedding planes and shale transiting from crumpled, mylonitized, and scaly structure to porphyritic and cataclastic structure) usually occurred in shale with a high calcium content. The shale with higher content of argillaceous and organic matters mostly showed the horizontal zoning pattern. From fold cores to limbs, shale gradually changed from crumpled, fractured-crumpled, and scaly structure to flaky and platy structure. In thick-bedded shale near core zones of folds, structural deformations were mainly characterized by bedding-parallel fractures, showing platy and cataclastic structure. The structural deformations of shale in core limbs were generally weak, and the thin-bedded shale mainly developed bedding-parallel fractures. Shale mostly showed platy and flaky structure.

Due to the intense tectonic compressions from south to north and from east to west during the geological history, the well-developed fold structures largely control the tectonic framework of the study area, which is characterized by the superposition of the E–W- and N–S-trending compressive structures (**Figure 1**). The near E–W-trending folds gradually weakened from south to north in terms of structural intensity and complex degree. Among the near N–S-trending folds, the anticlines were more closed and complex than the synclines, forming wide-spaced anticlines.

The large-scale faults were mainly distributed in the areas controlled by the Guanxingnan anticline and the Hetaowan anticline. The faults in the core zone of the Guanxingnan anticline are reverse faults. Although the faults observed in the south limb of the Hetaowan anticline show as normal faults nowadays, the fault planes of the main and secondary faults usually retained structural traces of reverse faults, such as the occurrence of fault planes, the porphyritic rock belts near the fault planes, and the development of drag folds (Cheng et al., 2021), indicating that the normal faults used to be reverse faults. According to the revealed distribution rules of TDSs on reverse faults, the shale near these faults should have experienced intense structural deformation and mainly displays strong deformation structures (crumpled, mylonitized, fractured-crumpled, scaly, flaky, and porphyritic structure), with bedding-parallel and crumpled cleavages well developed. From the fault planes to the south limb of the Hetaowan anticline, shale gradually transited into cataclastic and platy structure. The distribution belts of shale deformation structures should extend in near E–W direction.

The Guanxingnan anticline shows as a tight linear fold and is divided into two secondary tight folds at the eastern end. There should be strong deformation structures developed in the cores and core–limb transitional areas. The Hetaowan anticline shows as an anticlinorium with reverse faults and strike-slip faults well developed in the core and south limb. Shale near the fold core and reverse faults should display strong deformation structures. In the limbs and the areas controlled by strike-slip faults, shale should show medium-intensity brittle deformation structures (cataclastic and platy structure). The Dawuji syncline is relatively gentle. Shale deformation should be weak and mainly show weak brittle deformation structures and primary structure.

In the middle and north parts of the study area, large-scale faults are less developed and should have no considerable influences on shale deformation. The distribution of shale deformation structures is mainly controlled by fold structures. The NEE-trending folds in the middle and north regions (the Yunshanba syncline, the Taiyang anticline, and the Xuyong syncline) are generally wide and gentle. Shale should mainly show weak brittle deformation structures and primary structure. There might be medium-intensity brittle deformation structures (cataclastic and platy structure).

As for the N–S-trending fold structures, the Zhengdong anticline and Huangnizui anticline are significantly tight and closed than the Luobu syncline. Shale in the cores of the two mentioned anticlines should have experienced intense structural deformation and show crumpled, scaly, fractured-crumpled, and flaky structure. In the core–limb transitional areas of anticlines, there should be near N–S-trending brittle deformation belts, in which platy and cataclastic structure are well developed. By contrast, shale in the N–S-trending synclines and the limbs of N–S-trending anticlines should mainly display primary structure and weak brittle deformation structures.

CONCLUSION

Systematical structural deformation observations of shale outcrops were conducted to reveal the relationships between geological structures and shale deformation, based on which the distribution rules of various deformation structures were predicted. The following conclusions are drawn:

1) Shale near reverse faults usually showed complex folding deformations with dense and fine bedding-parallel and crumpled cleavages. Strong deformation structures (such as porphyritic, crumpled, mylonitized, scaly structure) were distributed. Shale near normal and strike-slip faults usually showed cataclastic structure. Shale deformation in areas controlled by folds can display vertical and parallel zoning patterns. In shale outcrops showing vertical pattern, structural deformation belts generally distributed along with bedding planes and shale deformation structures gradually transited from ductile and brittle-ductile transitional series to brittle ones from the main slip surfaces. In the shale outcrops of horizontal zoning pattern, shale deformation structures distributed along the axial surfaces of folds and shale generally transited from ductile and brittle-ductile transitional deformation structures to flaky and platy structure to the direction away from axial surfaces.
2) Due to the differences in strata structure, mineral composition, and physical properties, there were considerable differences in shale deformation between different shale sections of the same structural location. Under tectonic compressions, the thin-bedded shale (with dense and fine laminated structure) mostly showed stronger structural deformations than the medium–thick-bedded shale. Bedding-parallel and crumpled cleavages are usually more developed in the thin-bedded shale sections, resulting in strong shale deformation structures. The medium–thick-bedded shale usually showed cataclastic and platy structure.
3) Strong deformation structures were predicted to mainly distribute in the core zones of the anticlines and near the fault planes of reverse faults. In the core zones of gentle anticlines and synclines and the core–limb transitional areas of tight anticlines, the shale is supposed to show medium-intensity brittle deformation, such as platy and cataclastic structure. Shale in the limbs of anticlines and synclines and other structurally simple areas should mainly show primary structure and weak brittle deformation structures. Furthermore, it is predicted that the strong deformation belts and bedding slip surfaces were mainly distributed at these three sections: the bottom member of the Wufeng Formation, the bottom and upper members of the Longmaxi Formation.

DATA AVAILABILITY STATEMENT

The original contributions presented in the study are included in the article/**Supplementary Material**, and further inquiries can be directed to the corresponding author.

AUTHOR CONTRIBUTIONS

GC: Methodology, Investigation, Data curation and formal analysis, Writing–original draft. BJ: Methodology, Supervision, Funding acquisition, Writing–review and editing. FL: Visualization, Writing–review and editing. ML: Investigation, Supervision, Writing–review and editing. YS: Investigation, Sample collection, Data curation.

FUNDING

This research was sponsored by the National Science and Technology Major Project (grant numbers: 2017ZX05035004, 2016ZX05044001, KYCX21_2327) and the Postgraduate Research and Practice Innovation Program of Jiangsu Province (grant number: KYCX21_2327).

SUPPLEMENTARY MATERIAL

The Supplementary Material for this article can be found online at: https://www.frontiersin.org/articles/10.3389/feart.2022.813074/full#supplementary-material

REFERENCES

Burchfiel, B. C., Zhiliang, C., Yupinc, L., and Royden, L. H. (1995). Tectonics of the Longmen Shan and Adjacent Regions, central China. *Int. Geology. Rev.* 37, 661–735. doi:10.1080/00206819509465424

Carey, J. W., Lei, Z., Rougier, E., Mori, H., and Viswanathan, H. (2015). Fracture-permeability Behavior of Shale. *J. Unconventional Oil Gas Resour.* 11, 27–43. doi:10.1016/j.juogr.2015.04.003

Chen, B. (1998). Characteristics and Classification of Tectonite of Ductile Shear Deformation in Epimetamorphic Microclastic Rocks. *ATCA Petrol. Mineral.* 17 (1), 30–34. CNKI:SUN:YSKW.0.1998-01-004.

Cheng, G., Jiang, B., Li, M., Li, F., and Zhu, M. (2021). Structural Evolution of Southern Sichuan Basin (South China) and its Control Effects on Tectonic Fracture Distribution in Longmaxi Shale. *J. Struct. Geology.* 153, 104465. doi:10.1016/j.jsg.2021.104465

Cheng, G., Jiang, B., Li, M., Liu, J., and Li, F. (2020a). Effects of Pore Structure on Methane Adsorption Behavior of Ductile Tectonically Deformed Coals: An Inspiration to Coalbed Methane Exploitation in Structurally Complex Area. *J. Nat. Gas Sci. Eng.* 74, 103083. doi:10.1016/j.jngse.2019.103083

Cheng, G., Jiang, B., Li, M., Li, F., and Song, Y. (2020b). Effects of Pore-Fracture Structure of Ductile Tectonically Deformed Coals on Their Permeability: An Experimental Study Based on Raw Coal Cores. *J. Pet. Sci. Eng.* 193, 107371. doi:10.1016/j.petrol.2020.107371

Chester, F. M., Friedman, M., and Logan, J. M. (1985). Foliated Cataclasites. *Tectonophysics* 111, 139–146. doi:10.1016/0040-1951(85)90071-X

Curtis1, J. B. (2002). Fractured Shale-Gas Systems. *Bulletin* 86, 1921–1938. doi:10.1306/61EEDDBE-173E-11D7-8645000102C1865D

Deville, E., Dutrannoy, C., Schmitz, J., Vincent, B., Kohler, E., and Lahfid, A. (2020). Shale Tectonic Processes: Field Evidence from the Parras Basin (north-eastern Mexico). *Mar. Pet. Geology.* 122, 104688. doi:10.1016/j.marpetgeo.2020.104688

Eichhubl, P., D'Onfro, P. S., Aydin, A., Waters, J., and McCarty, D. K. (2005). Structure, Petrophysics, and Diagenesis of Shale Entrained along a normal Fault at Black Diamond Mines, California-Implications for Fault Seal. *Bulletin* 89 (9), 1113–1137. doi:10.1306/04220504099

Engelder, J. T. (1974). Cataclasis and the Generation of Fault Gouge. *Geol. Soc. America Bull.* 85, 1515–1522. doi:10.1130/0016-7606(1974)85<1515:catgof>2.0.co;2

Fengli, L., Bo, J., Guoxi, C., Yu, S., and Zheng, T. (2019). Structural and Evolutionary Characteristics of Pores-Microfractures and Their Influence on Coalbed Methane Exploitation in High-Rank Brittle Tectonically Deformed Coals of the Yangquan Mining Area, Northeastern Qinshui basin, China. *J. Pet. Sci. Eng.* 174, 1290–1302. doi:10.1016/j.petrol.2018.11.081

Gou, Q., Xu, S., Hao, F., Yang, F., Shu, Z., and Liu, R. (2021). The Effect of Tectonic Deformation and Preservation Condition on the Shale Pore Structure Using Adsorption-Based Textural Quantification and 3D Image Observation. *Energy* 219, 119579. doi:10.1016/j.energy.2020.119579

Gu, Y., He, J., Xu, S., Tian, Q., Zhang, W., and Yin, S. (2020). Influence of Differential Structural Deformation on Shale Reservoirs: a Case Study of the Lower Silurian Longmaxi Shale in north Guizhou, Southern China. *Geol. Mag.* 158, 673–684. doi:10.1017/S0016756820000771

Gu, Z., Wang, X., Nunns, A., Zhang, B., Jiang, H., Fu, L., et al. (2021). Structural Styles and Evolution of a Thin-Skinned Fold-And-Thrust belt with Multiple Detachments in the Eastern Sichuan Basin, South China. *J. Struct. Geology.* 142, 104191. doi:10.1016/j.jsg.2020.104191

Guo, T. (2013). Evaluation of Highly Thermally Mature Shale-Gas Reservoirs in Complex Structural Parts of the Sichuan Basin. *J. Earth Sci.* 24 (6), 863–873. doi:10.1007/s12583-013-0384-4

Guo, T., and Zeng, P. (2015). The Structural and Preservation Conditions for Shale Gas Enrichment and High Productivity in the Wufeng-Longmaxi Formation, Southeastern Sichuan Basin. *Energy Exploration & Exploitation* 33, 259–276. doi:10.1260/0144-5987.33.3.259

Guoxi, C., Bo, J., Ming, L., Fengli, L., and Shaochun, X. (2020). Quantitative Characterization of Fracture Structure in Coal Based on Image Processing and Multifractal Theory. *Int. J. Coal Geology.* 228, 103566. doi:10.1016/j.coal.2020.103566

Hatcher, R. D., Jr. (1978). Comment and Reply on 'Eastern Piedmont Fault System: Speculations on its Extent'. *Geol* 6, 580–582. doi:10.1130/0091-7613(1978)6<580b:caroep>2.0.co;2

Jiang, B., and Ju, Y. (2004). Tectonic Coal Structure and its Petro-Physical Features. *Nat. Gas. Ind.* 24 (5), 27–29. doi:10.3321/j.issn:1000-0976.2004.05.009

Jiang, B., Qu, Z., Wang, G. G. X., and Li, M. (2010). Effects of Structural Deformation on Formation of Coalbed Methane Reservoirs in Huaibei coalfield, China. *Int. J. Coal Geology.* 82, 175–183. doi:10.1016/j.coal.2009.12.011

Ju, Y., Jiang, B., Hou, Q., and Wang, G. (2004). The New Structure-Genetic Classification System in Tectonically Deformed Coals and its Geological Significance. *J. China Coal Soc.* 29 (5), 513–517. doi:10.3321/j.issn:0253-9993.2004.05.001

Ju, Y., Sun, Y., Tan, J., Bu, H., Han, K., Li, X., et al. (2018). The Composition, Pore Structure Characterization and Deformation Mechanism of Coal-Bearing Shales from Tectonically Altered Coalfields in Eastern China. *Fuel* 234 (15), 626–642. doi:10.1016/j.fuel.2018.06.116

Katori, T., Shigematsu, N., Kameda, J., Miyakawa, A., and Matsumura, R. (2021). 3D Fault-Zone Architecture across the Brittle-Plastic Transition along the Median Tectonic Line, SW Japan: Fault-Rock Characterization. *J. Struct. Geology.* 153, 104446. doi:10.1016/j.jsg.2021.104446

Li, X., Zhu, H., Zhang, K., Li, Z., Yu, Y., Feng, X., et al. (2021). Pore Characteristics and Pore Structure Deformation Evolution of Ductile Deformed Shales in the Wufeng-Longmaxi Formation, Southern China. *Mar. Pet. Geology.* 127 (12), 104992. doi:10.1016/j.marpetgeo.2021.104992

Li, Z., Jiang, Z., Liang, Z., Yu, H., and Yang, Y. (2019). Pore-structure Characterisation of Tectonically Deformed Shales: a Case Study of Wufeng-Longmaxi Formation in Western Hunan Province, Southern China. *Aust. J. Earth Sci.* 66 (7), 1075–1084. doi:10.1080/08120099.2019.1588168

Liang, M., Wang, Z., Gao, L., Li, C., and Li, H. (2017). Evolution of Pore Structure in Gas Shale Related to Structural Deformation. *Fuel* 197, 310–319. doi:10.1016/j.fuel.2017.02.035

Liang, M., Wang, Z., Li, C., Li, H., Zhang, L., Feng, X., et al. (2020). Effect of Structural Deformation on Permeability Evolution of marine Shale Reservoirs. *J. Geomech.* 26 (6), 840–851. doi:10.12090/j.issn.1006–6616.2020.26.06.066(Chinese with English abstract)

Liu, S., Deng, B., Sun, W., and Li, Z. (2012). Architecture of basin-mountain Systems and Their Influences on Gas Distribution: A Case Study from the Sichuan basin, South China. *J. Asian Earth Sci.* 47, 204–215. doi:10.1016/j.jseaes.2011.10.012

Liu, S., Deng, B., Zhong, Y., Ran, B., Yong, Z., Sun, W., et al. (2016). Unique Geological Features of Burial and Superimposition of the Lower Paleozoic Shale Gas across the Sichuan Basin and its Periphery. *Earth Sci. Front.* 23 (1), 11–28. doi:10.13745/j.esf.2016.01.002(Chinese with English abstract)

Ma, Y., Zhong, N., Han, H., Li, D., Zhang, Y., and Cheng, L. (2014). Definition and Sturcture Characteristics of Pores in Mylonitized Organic-Rich Shales. *Sci. China Earth Sci.* 57, 3027–3034. doi:10.1007/s11430-014-4968-3

Ma, Y., Ardakani, O. H., Zhong, N., Liu, H., Huang, H., Larter, S., et al. (2020). Possible Pore Structure Deformation Effects on the Shale Gas Enrichment: an Example from the Lower Cambrian Shales of the Eastern Upper Yangtze Platform, south China. *Int. J. Coal Geology.* 217, 103349. doi:10.1016/j.coal.2019.103349

Marshark, S., and Mitra, G. (1988). *Basic Methods of Structural Geology*. New Jersay: Prentice-Hall.

Pan, J., Zhao, Y., Hou, Q., and Jin, Y. (2015). Nanoscale Pores in Coal Related to Coal Rank and Deformation Structures. *Transp Porous Med.* 107 (2), 543–554. doi:10.1007/s11242-015-0453-5

Shang, F., Zhu, Y., Gao, H., Wang, Y., and Liu, R. (2020). Relationship between Tectonism and Composition and Pore Characteristics of Shale Reservoirs. *Geofluids* 2020, 1–14. doi:10.1155/2020/9426586

Sibson, R. H. (1977). Fault Rocks and Fault Mechanisms. *J. Geol. Soc.* 133, 191–213. doi:10.1144/gsjgs.133.3.0191

Wang, X., Wang, Z., and Li, J. (1982). Basic Characteristics of Tectonites in Southern Tancheng-Lujiang Fault Zone. *Bull. Geomech. Cags* 3, 141–153. & 197–198. (Chinese with English abstract). Available at: https://www.cnki.com.cn/Article/CJFDTotal-DZLX198203011.htm.

Wei, G., Jia, D., Yang, W., Xiao, A., Wang, L., and Wu, L. (2019). *Structural Characteristics, Oil and Gas in Sichuan Basin*. Beijing: Science Press.

Woodcock, N. H., and Mort, K. (2008). Classification of Fault Breccias and Related Fault Rocks. *Geol. Mag.* 145, 435–440. doi:10.1017/S0016756808004883

Xiao, X.-M., Wei, Q., Gai, H.-F., Li, T.-F., Wang, M.-L., Pan, L., et al. (2015). Main Controlling Factors and Enrichment Area Evaluation of Shale Gas of the Lower Paleozoic marine Strata in south China. *Pet. Sci.* 12, 573–586. doi:10.1007/s12182-015-0057-2

Zheng, Y., Liao, Y., Wang, Y., Xiong, Y., and Peng, P. a. (2018). Organic Geochemical Characteristics, Mineralogy, Petrophysical Properties, and Shale Gas Prospects of the Wufeng-Longmaxi Shales in Sanquan Town of the Nanchuan District, Chongqing. *Bulletin* 102 (11), 2239–2265. doi:10.1306/04241817065

Zhong, Z. (1994). Developments in Tectonite Study. *Earth Sci. Front.* 1 (1–2), 162–169. (Chinese with English abstract)) Available From: https://www.doc88.com/p-6049774429421.html?r=1.

Zhu, D., and Wang, Z. (1995). Genetic Classification and Nomenclature of Tectonites Based on Textures. *Bull. Geomech. Cags* 16, 55–76. (Chinese with English abstract) Available From: https://www.docin.com/p-1097672244.html, http://www.cnki.com.cn/Article/CJFDTotal-DZLX199400005.htm.

Zhu, H., Ju, Y., Qi, Y., Huang, C., and Zhang, L. (2018). Impact of Tectonism on Pore Type and Pore Structure Evolution in Organic-Rich Shale: Implications for Gas Storage and Migration Pathways in Naturally Deformed Rocks. *Fuel* 228, 272–289. doi:10.1016/j.fuel.2018.04.137

Zhu, H., Ju, Y., Huang, C., Han, K., Qi, Y., Shi, M., et al. (2019). Pore Structure Variations across Structural Deformation of Silurian Longmaxi Shale: an Example from the Chuandong Thrust-fold belt. *Fuel* 241, 914–932. doi:10.1016/j.fuel.2018.12.108

Zhu, H., Ju, Y., Sun, Y., Huang, C., Feng, H., Raza, A., et al. (2021). Evolution Characteristics and Models of Shale Pores and Fractures under Tectonic Deformation: A Case Study of the Lower Paleozoic marine Shale in the Sichuan Basin and its Periphery. *Oil Gas Geol.* 42 (1), 186–200. doi:10.11743/ogg20210116

Conflict of Interest: The authors declare that the research was conducted in the absence of any commercial or financial relationships that could be construed as a potential conflict of interest.